Determining the elastic properties of aptamer-ricin single molecule multiple pathway interactions

Bin Wang, Bosoon Park, Yongkuk Kwon, and Bingqian Xu'

Citation: Appl. Phys. Lett. **104**, 193702 (2014); doi: 10.1063/1.4876603
View online: http://dx.doi.org/10.1063/1.4876603
View Table of Contents: http://aip.scitation.org/toc/apl/104/19
Published by the American Institute of Physics

Determining the elastic properties of aptamer-ricin single molecule multiple pathway interactions

Bin Wang,[1] Bosoon Park,[2] Yongkuk Kwon,[3] and Bingqian Xu[1,a)]
[1]*Single Molecule Study Laboratory, College of Engineering and Nanoscale Science and Engineering Center, University of Georgia, Athens, Georgia 30602, USA*
[2]*USDA-ARS, Russell Research Center, Athens, Georgia 30605, USA*
[3]*Avian Disease Division, Animal Plant and Fisheries Quarantine and Inspection Agency, Anyang, South Korea*

(Received 14 March 2014; accepted 30 April 2014; published online 13 May 2014)

We report on the elastic properties of ricin and anti-ricin aptamer interactions, which showed three stable binding conformations, each of which has its special elastic properties. These different unbinding pathways were investigated by the dynamic force spectroscopy. A series-spring model combining the worm-like-chain model and Hook's law was used to estimate the apparent spring constants of the aptamer and linker molecule polyethylene glycol. The aptamer in its three different unbinding pathways showed different apparent spring constants. The two reaction barriers in the unbinding pathways also influence the apparent spring constant of the aptamer. This special elastic behavior of aptamer was used to distinguish its three unbinding pathways under different loading rates. This method also offered a way to distinguish and discard the non-specific interactions in single molecule experiments. © *2014 AIP Publishing LLC*. [http://dx.doi.org/10.1063/1.4876603]

Elasticity of biomolecules plays important roles in many cellular activities, and most of these reactions and pathways depend on the molecular motions and fluid behaviors of biomolecules with their specific elastic properties.[1,2] Although some theoretical and experimental methods have been developed to investigate the elasticity of nucleic acids and proteins, most DNAs and some proteins inherently act as flexible and elastic ligand and receptor with complex behaviors, which make it difficult to study their reaction mechanisms.[3–5] Among all types of DNA molecules currently studied, aptamer has been considered as a versatile tool for biomedical and biosensing applications.[6] Aptamer refers to short single strand DNA or RNA sequences that have specific interactions with other biomolecules.[6] The specific biochemical properties and relatively low cost have made aptamer a widely used regent in both fundamental research and practical applications.[5–9] However, aptamers have shown complex biophysical and biochemical behaviors, such as multiple binding sites and multiple reaction pathways. In order to understand the complex elastic properties of aptamers during their reactions, a feasible method that allows the measurements of the detailed reaction properties quantitatively is highly required.[10–13]

Atomic force microscopy (AFM) and dynamic force spectroscopy (DFS) have been used to experimentally determine mechanical and elastic properties of biospecies such as DNA and protein at nanometer level.[14–16] In theoretical studies, Bell-Evans model, worm-like chain (WLC) model, and Hook's law have been used to explain the elastic behaviors of DNAs or proteins.[13,17–19] Great efforts have been made to study the behaviors of single DNA molecule under stretching.[20–23] However, little is known about elastic behaviors of DNA during their unbinding processes because of the complexity of the DNA binding structures and biophysical properties.[24] In this study, we revealed the single molecule elastic properties from the experimentally measured AFM data, and developed a relatively simple and practical elasticity model to quantitatively explain the elastic behaviors of ssDNA during the single molecule binding/unbinding reaction.

This practical elasticity model is based on the DFS measured extension distributions of each unbinding pathway under a wide range of force loading rates. The DFS experimental setup and series-spring model are schematically shown in Fig. 1. A polyethylene glycol (PEG) chain with molecular weight of 2000, PEG2000, was used as linker and spacer to connect aptamer to the gold coated AFM tip surface.[25] The PEG2000 was treated as an elastic polymer molecule in solvent, and its physical behaviors follow WLC model.[26] The aptamer formed a stable folding structure in PBS buffer, and the applied force will distort and break the connection between aptamer and ricin during the unbinding process. Therefore, their elastic behaviors cannot be studied by a simple WLC model. The ricin protein is simplified as a rigid receptor and molecular docking simulations predicted that it has three binding site for the aptamer (Fig. 1(b)). Overall, a series-spring model was established to describe this multiple-pathway system (Fig. 1(a)).

The molecular basis of the elastic properties in different pathways is that each reaction pathway has its corresponding binding residues on aptamer and ricin surface. The HADDOCK docking simulation and Amber molecular dynamics (MD) simulation showed that the aptamer and ricin can form three stable binding conformations. Figs. S1(b), S1(c), and S1(d)[27] illustrate the predicted active residues for each ricin-aptamer binding conformation.[28,29] Although their binding areas on ricin surface have overlap, the aptamer binding conformations and ricin active residues have significant differences, as shown in Figs. S1(b), S1(c), and S1(d).[27] Moreover, for the two-loop binding pathway, the predicted ricin binding residues are not simply the sum of the ones for individual loop binding. Indeed, the simulations results

a)Email: bxu@engr.uga.edu

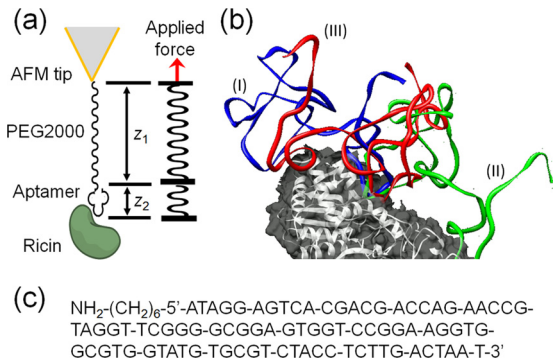

FIG. 1. The force-extension model for the aptamer-ricin interactions. (a) The series-spring model. (b) The simulated aptamer-ricin binding conformations, where the aptamer conformations are labeled as (I) for pathway 1, (II) for pathway 2, and (III) for pathway 3. (c) The sequence of the aptamer modified with amino functional group.

indicate that three reaction pathways should have different chemomechanical properties, which is confirmed by the DFS experimental data. Force histograms (Fig. S2) and extension histograms (Fig. S3)[27] suggested that the unbinding reactions can happen through three pathways. The pathway 1 (labeled as binding conformation (I) in Fig. 1(b)) happens between ricin and aptamer loop#3, as shown in Fig. S1(c),[27] with the small "most probable unbinding extension value" in each extension histogram (peak 1 in Figs. 2(a) and 2(b)). The pathway 2 (labeled as binding conformation (II) in Fig. 1(b)) happens between ricin and loop#1, as shown in Fig. S1(b).[27] The pathway 3 (labeled as binding conformation (III) in Fig. 1(b)) happens between ricin and loop#1-loop#3 simultaneously, as shown in Fig. S1(d).[27] The pathways 1 and 2 have different most probable unbinding force values (Figs. S2(a) to S2(e)),[27] but the most probable extension values are very similar and merged to one peak (peak 2 in Figs. 2(a) and 2(b)) in the extension histogram. These experimental data indicate that PEG2000 linker and aptamer have their specific elastic properties during the binding-unbinding processes through different pathways.

We measured the force-extension curves under three ranges of loading rates (examples shown in Fig. 2) and used 250 curves to construct both the force and extension histograms for each loading rate. Under low loading rate 0.24 nN/s, 2.72 nN/s, 15.37 nN/s, 38.02 nN/s, and 51.64 nN/s, the force histograms showed three peaks (Figs. S2(a) to S2(e)), and the extension histograms showed two peaks (Figs. S3(a) to S3(e)).[27] Under medium loading rates 82.06 nN/s and 100 nN/s, force histograms showed two peaks (Under high loading rates 200 nN/s, 400 nN/s, and 600 nN/s (Figs. S2(h) to S2(j), Figs. S3(h) to S3(j)),[27] only one peak was observed in both the force histograms and extension histograms.

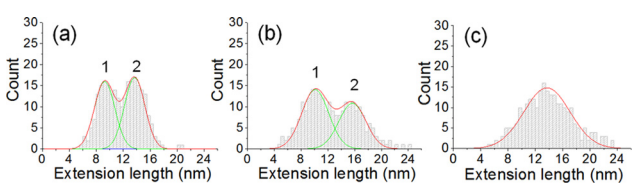

FIG. 2. The representative extension histograms under different loading rates. (a) 0.24 nN/s. (b) 51.64 nN/s. (c) 400.00 nN/s.

For the PEG2000 linker molecule (as part of the series-spring model in Fig. 1(a)), a modified WLC model was used to fit the stretching of PEG2000 in the force-extension curves.[26] The contour length of 15 nm, persistence length of 0.38 nm, and enthalpic correction of 1561 pN were used for the extended WLC model of PEG2000[26] and directly adopted in our calculations. Tables S1 and S2[27] showed the simulations of PEG extension, spring constant (k_{PEG}) calculations, and experimentally measured extension values under different loading rates.

Based on the series-spring model in Fig. 1(a), the total extension z is the sum of PEG extension (z_1) and aptamer extension (z_2) under the same unbinding force. Therefore, we can estimate the apparent spring constant of aptamer (k_{apt}) during the entire stretching and unbinding process, and this parameter is directly related to the three unbinding pathways. If we ignore any detailed structural and environmental effects, the k_{PEG}, k_{apt}, unbinding force f, and total extension z_{total} should follow the relationships in the series springs:

$$z_1 = f_{PEG} \times k_{PEG}, \tag{1}$$

$$z_2 = f_{apt} \times k_{apt}, \tag{2}$$

$$f_{PEG} = f_{apt}, \tag{3}$$

$$z_{total} = z_1 + z_2. \tag{4}$$

The k_{PEG} and k_{apt} values estimated by this series-spring model are listed in Table I. The details of these calculations were shown in Tables S1 and S2.[27] Under low and medium loading rates, the PEG in WLC model showed increasing k_{PEG} values with the increase of force.[26] For the aptamer, different unbinding pathways showed their corresponding k_{apt} values, which were not affected by the changes of loading rates. This phenomenon is especially very clear for pathway 2 through a wide range of loading rate, which indicates that the aptamer binding conformation in this pathway showed very consistent elastic properties during the unbinding reaction.

The data from Table I were also used to study the influence of different unbinding pathways on the elastic properties of PEG and aptamer. Pathway 1 can be clearly distinguished with the force histograms (Fig. S2) and extension histograms (Fig. S3),[27] but the aptamer did not show a consistent k_{apt} value under different loading rates. Under lowest loading rates 0.24 nN/s, 2.72 nN/s, and 15.37 nN/s, the estimated aptamer extensions continued to decrease until it is even smaller than the WLC extension of PEG2000 (Table S1).[27] One reason is that the errors of the measured unbinding forces will significantly increase from a combination effect of lower loading rates (e.g., 10 nN/s) and longer linker molecule.[22] Here, the linker PEG2000 is about 15 nm, which can cause significant errors in the measured force values, and in turn lead to the large errors in the estimated PEG extension values. Therefore, the simulated PEG extension values in Tables S1 and S2[27] could be overestimated. Another reason for the large error is that the interaction through pathway 1 was so week that it was easily interfered by the errors from the experimental measurements. The aptamer in pathway 1 always showed the smallest unbinding

TABLE I. The estimated spring constants for PEG2000 and aptamer molecules.

Loading rate (nN/s)	PEG spring constant k_{PEG} (N/m)			Aptamer spring constant k_{apt} (N/m)		
Outer barrier pathway	1	2	3	1	2	3
0.24	0.007	0.029	0.085	0.101	0.020	0.061
2.72	0.008	0.029	0.108	0.450	0.019	0.066
15.37	0.011	0.052	0.161	N/A[a]	0.025	0.062
38.02	0.012	0.054	0.194	N/A[a]	0.021	0.054
51.64	0.012	0.062	0.336	N/A[a]	0.019	0.047
82.06	0.021	0.079	N/A[b]	N/A[a]	0.019	N/A[b]
100.00	0.029	0.089	N/A[b]	N/A[a]	0.020	N/A[b]
Inner barrier pathway						
200.00	0.179			0.417		
400.00	0.250			0.405		
600.00	0.447			0.442		

[a]The estimated z_1 is longer than the measured z_{total}, the series-spring model is not valid here.
[b]The force histograms under loading rates 82.06 nN/s and 100.00 nN/s did not show pathway 3.

force value under each loading rate. Therefore, the energy barrier for the unbinding process through pathway 1 is always the lowest compared to other pathways under the same loading rate. The PEG extension to overcome this low energy barrier (z_1) dominated the elastic process in pathway 1, and the aptamer extension (z_2) became comparable to the thermal noise in DFS measurements. According to the calculations in Table S1,[27] the z_2 values for pathway 1 became invalid under relatively larger loading rates, which are mainly caused by the two reasons mentioned above.

On the contrary, based on molecular dynamics and docking simulations, the aptamer in pathway 2 and 3 show more contact areas to ricin surface (Fig. 1(b)), which indicate that the unbinding forces generated from these two pathways were large enough to dominate the extension measurements. Consequently, these two pathways showed very consistent z_2 values under different loading rates, and in turn maintained very consistent k_{apt} values in a large range of loading rates (Tables S1 and S2).[27]

Overall, the calculations of k_{apt} values from the extension distributions are consistent with our multiple-barrier multiple-pathway model and can be used to distinguish the three pathways. The disagreement between the aptamer spring constants calculations for Pathway 1 and the ones for other pathways showed the limitation of the series-spring elasticity model, which works well for certain experimental conditions and aptamer conformations. However, the multiple-pathway model is still valid for all of the experimental histograms in Figs. S2 and S3.[27] The k_{apt} for pathway 2 fitted the series-spring model best in a large range of loading rates. The k_{apt} for pathway 3 showed the same consistency as long as it existed in force histograms under low loading rates. Under the high loading rates, the unbinding processes happened through a new pathway with different unbinding energy barrier,[30] and the three-pathway model will not be valid any more. Overall, these consistent k_{apt} values for their corresponding pathways proved that the aptamer-ricin complex has its specific elastic properties for different unbinding pathways. The k_{apt} values can be used as a special elastic parameter to distinguish different unbinding pathways under proper experimental conditions.

To test the reliability of these estimated spring constants for different pathways, we simulated the force-extension curves using the series-spring model in Fig. 1(a). The unbinding force value was set by the measured force-extension curve, and the estimated k_{apt} values of the three pathways were used to construct their corresponding total extension values. Finally, the experimental extension value was compared with the simulated ones, and classified into one of the three pathways. The comparison of experimental force-extension curves and the simulated ones under loading rate 51.64 nN/s are shown in Fig. 3. The representative f-d curves under other loading rates are shown in Fig. S4. Under each loading rate, the experimental curve (black) was compared with three simulated curves constructed for their corresponding pathways. When k_{apt} value was not available, the simulated PEG extension curve was used to represent the total extension. These experimental curves can be called "the most probable curves" for their corresponding pathways. For example, the experimental curve in Fig. 3(b) (black) fits both force and extension values of the simulated curve for pathway 2 (green, labeled as II), which indicates that this experimental curve is the most probable unbinding curve for pathway 2 under 51.64 nN/s.

The standard deviation ($\pm 1\sigma$) of each Gaussian fitting peak in Fig. 2 was used to classify each experimental force-extension curve into a certain pathway or into the "unknown" group. Some experimental curves have the extension values drifting so far away that the difference between the measured extension and any of the three simulated extension is larger than 1σ. Those curves were classified as "unknown" for each

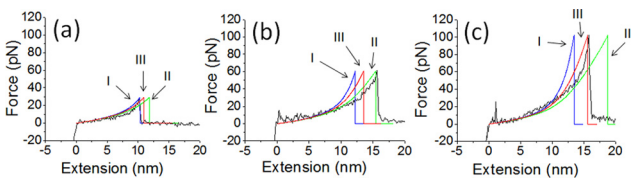

FIG. 3. Representative experimental and simulated force-extension curves under 51.64 nN/s. For each experimental curve in (a), (b), and (c), I, II, and III labeled the simulated curves for pathway 1, pathway 2, and pathway 3, respectively.

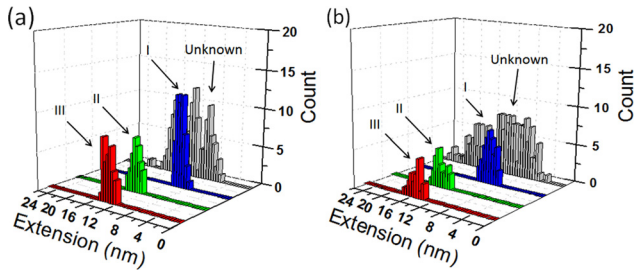

FIG. 4. The reconstitutions of original extension histograms under two representative loading rates (a) 0.24 nN/s and (b) 82.06 nN/s. In each 3-D histogram, from the front to the back, are the new extension histograms for the most probable curves for pathway 3 (labeled as III), pathway 2 (labeled as II), pathway 1 (labeled as I), and the unknown group (labeled as "Unknown").

loading rate. After each individual force-extension curve was checked, a new histogram was made to show the curves distributions for the three pathways and unknown groups under the same loading rate (Fig. 4). For example, under loading rate 0.24 nN/s, 97 out of 250 force-extension curves can be classified into one of the three unbinding pathways. Among them, 43 curves were classified into pathway 1 (labeled as I), 30 curves were classified into pathway 2 (labeled as II), and 24 curves were classified into pathway 3 (labeled as III). The rest 153 curves were classified into unknown group, labeled as "Unknown" in Fig. 4(a). Therefore, 61% (153) of the f-d curves can not be determined to a certain pathway by this analysis. That ratio is larger than the one simply determined by 1σ deviation of the extension histogram ($1 - 68\% = 32\%$). Overall, the combination of force and extension as the criteria can put more curves to the unknown group, which indicates those curves may not be specific for any ricin-aptamer unbinding pathway. The uncertainty for the remaining curves was greatly reduced and can be used more confidently as specific f-d curves for ricin-aptamer interactions.

The method we developed here can be used to distinguish the specific unbinding pathways for individual force-extension curves measured in a multiple-pathway system. Although analysis may be limited by thermal noise, errors caused by linker molecule, and certain binding conformations, the experimental data and theoretical simulations agreed with each other in a relatively simple series-spring elasticity model. The principles used in this model can be applied to the studies of other systems with multiple unbinding pathways, such as the interactions of biomolecules on cell surface or protein-nucleic acid interactions involved in cellular activities, where the non-specific interaction is always a serious issue for data analysis. With the help of this approach, DFS force-extension curves for a specific biophysical process or reaction pathway can be selected by its corresponding elastic parameters, while the uncertainty in the results of single molecule experiments can be significantly reduced.

We thank National Science Foundation (ECCS 1231967 and CBET 1139057) for financial support of this research.

[1]E. M. Puchner and H. E. Gaub, Annu. Rev. Biophys. **41**, 497 (2012).
[2]K. A. Melzak, S. Moreno-Flores, A. E. Lopez, and J. L. Toca-Herrera, Soft Matter **7**, 332 (2011).
[3]L. Saiz, J. Phys.: Condens. Matter **24**, 193102 (2012).
[4]C.-Y.Chen, T.-Y. Chien, C.-K. Lin, C.-W. Lin, Y.-Z. Weng, and D. T.-H. Chang, PLoS ONE **7**, e30446 (2012).
[5]Z. Xie, S. Hu, J. Qian, S. Blackshaw, and H. Zhu, Cell. Mol. Life Sci. **68**, 1657 (2011).
[6]Y. Nakamura, Adv. Polym. Sci. **249**, 135 (2012).
[7]B. Dey, S. Thukral, S. Krishnan, M. Chakrobarty, S. Gupta, C. Manghani, and V. Rani, Mol. Cell. Biochem. **365**, 279 (2012).
[8]A. D. Keefe, S. Pai, and A. Ellington, Nat. Rev. Drug Discovery **9**, 537 (2010).
[9]L. A. Liu and P. Bradley, Curr. Opin. Struct. Biol. **22**, 397 (2012).
[10]D. H. Paik and T. T. Perkins, Angew. Chem., Int. Ed. **51**, 1811 (2012).
[11]C. Hyeon and D. Thirumalai, J. Chem. Phys. **137**, 055103 (2012).
[12]A. V. Dobrynin, J.-M. Y. Carrillo, and M. Rubinstein, Macromolecules **43**, 9181 (2010).
[13]S. Kumar and G. Mishra, Soft Matter **7**, 4595 (2011).
[14]S. Kasas and G. Dietler, Eur. J. Physiol. **456**, 13 (2008).
[15]N. E. Kurland, Z. Drira, and V. K. Yadavalli, Micron **43**, 116 (2012).
[16]S. Kasas, G. Longo, and G. Dietler, J. Phys. D: Appl. Phys. **46**, 133001 (2013).
[17]G. I. Bell, Science **200**, 618 (1978).
[18]J. F. Marko and E. D. Siggia, Macromolecules **28**, 8759 (1995).
[19]R. G. Haverkamp, A. T. Marshall, and M. A. K. Williams, Phys. Rev. E **75**, 021907 (2007).
[20]S. Cui, Y. Yu, and Z. Lin, Polymer **50**, 930 (2009).
[21]M. Manghia, N. Destainville, and J. Palmerib, Eur. Phys. J. E **35**, 110 (2012).
[22]C. Ray, J. R. Brown, and B. B. Akhremitchev, J. Phys. Chem. B **111**, 1963 (2007).
[23]S. Guo, N. Lad, C. Ray, and B. B. Akhremitchev, Biophys. J. **96**, 3412 (2009).
[24]M. Ritzefeld, V. Walhorn, D. Anselmetti, and N. Sewald, Amino Acids **44**, 1457 (2013).
[25]B. Wang, C. Guo, G. Chen, B. Park, and B. Xu, Chem. Commun. **48**, 1644 (2012).
[26]F. Kienberger, V. P. Pastushenko, G. Kada, H. J. Gruber, C. Riener, H. Schindler, and P. Hinterdorfer, Single Mol. **1**, 123 (2000).
[27]See supplemental material at http://dx.doi.org/10.1063/1.4876603 for the docking simulation results, the force histograms and extension histograms under all loading rates, the calculations of apparent spring constants for PEG and aptamer under all loading rates, the comparisons of experimental f-d curves and simulated f-d curves under all loading rate, and the method used to establish the multiple peaks in the extension histograms.
[28]S. J. de Vries, M. van Dijk, and A. M. J. J. Bonvin, Nat. Protoc. **5**, 883 (2010).
[29]D. A. Case, T. A. Darden, T. E. Cheatham III, C. L. Simmerling, J. Wang, R. E. Duke, R. Luo, M. Crowley, R. C. Walker, W. Zhang, K. M. Merz, B. Wang, S. Hayik, A. Roitberg, G. Seabra, I. Kolossvary, K. F. Wong, F. Paesani, J. Vanicek, J. Liu, X. Wu, S. R. Brozell, T. Steinbrecher, H. Gohlke, Q. Cai, X. Ye, J. Wang, M.-J. Hsieh, G. Cui, D. R. Roe, D. H. Mathews, M. G. Seetin, C. Sagui, V. Babin, T. Luchko, S. Gusarov, A. Kovalenko, and P. A. Kollman, AMBER 11, University of California, San Francisco, 2010.
[30]B. Wang and B. Xu, Phys. Rev. E **89**, 022720 (2014).